

# Surrogate-based Bayesian calibration methods for climate models: a comparison of traditional and non-traditional approaches. \*

Maike F. Holthuijzen<sup>†</sup>   Atlanta Chakraborty<sup>‡</sup>   Elizabeth Krath<sup>†</sup>  
 Tommie Catanach<sup>†</sup>

## Abstract

Parameter calibration is crucial for reducing uncertainty and improving simulation accuracy in physics-based models, yet computational constraints pose significant challenges. Bayesian calibration methods offer a principled framework for combining prior knowledge with data while rigorously quantifying uncertainty. In this work, we compare four emulator-based Bayesian calibration methods—Calibrate-Emulate-Sample (CES), History Matching (HM), Bayesian Optimal Experimental Design (BOED), and a novel Goal-Oriented BOED (GBOED) approach—using the Lorenz '96 multiscale system as a testbed. Our GBOED formulation explicitly targets calibration-relevant quantities and leverages information-theoretic criteria for data selection. We assess each method in terms of calibration accuracy, uncertainty quantification, computational cost, and convergence behavior. We evaluate each method's performance in balancing computational cost, implementation complexity, and uncertainty quantification (UQ), with additional insights into convergence behavior as model evaluations increase. We find CES offers excellent performance but at high computational expense, while GBOED achieves comparable accuracy using fewer model evaluations. Standard BOED underperforms with respect to calibration accuracy, and HM shows moderate effectiveness but can be useful as a precursor. Our results highlight trade-offs among Bayesian strategies and demonstrate the promise of goal-oriented design in calibration workflows.

---

\*This material is based upon work supported by the U.S. Department of Energy, Office of Science, Office of Advanced Scientific Computing and Sandia National Laboratories Advanced Science and Technology Laboratory Directed Research and Development program. Sandia National Laboratories is a multimission laboratory managed and operated by National Technology and Engineering Solutions of Sandia, LLC., a wholly owned subsidiary of Honeywell International, Inc., for the U.S. Department of Energy's National Nuclear Security Administration under contract DE-NA0003525. This paper describes objective technical results and analysis. Any subjective views or opinions that might be expressed in the paper do not necessarily represent the views of the U.S. Department of Energy or the United States Government. This research used resources of the National Energy Research Scientific Computing Center (NERSC), a U.S. Department of Energy Office of Science User Facility located at Lawrence Berkeley National Laboratory, operated under Contract No. DE-AC02-05CH11231 using NERSC award DOE-ERCAPm3876. This research was supported in part through computational resources and services provided by Advanced Research Computing at the University of Michigan, Ann Arbor. The authors report there are no competing interests to declare.

<sup>†</sup>Sandia National Laboratories ( [mfholth@sandia.gov](mailto:mfholth@sandia.gov), [ekrath@sandia.gov](mailto:ekrath@sandia.gov), [tacatan@sandia.gov](mailto:tacatan@sandia.gov) )

<sup>‡</sup>University of Michigan, Dept. of Mechanical Engineering, Ann Arbor, MI 48109 ( [atlantac@umich.edu](mailto:atlantac@umich.edu) )

**Keywords.** Bayesian calibration, climate model, Bayesian optimal experimental design, history matching, CES, Gaussian process emulator, surrogate modeling

# 1 Introduction

Uncertainty quantification (UQ) plays a crucial role in validating computational models, particularly in climate science and other physics-based systems where predictions influence critical decision-making. Many-query problems, such as the calibration of expensive physics models, require repeated evaluations of complex simulations, making UQ both essential and computationally challenging. In these settings, calibration involves estimating uncertain model parameters, propagating their uncertainty through the system, and assessing the reliability of predictions. To be practically useful, UQ methods for calibration must not only be accurate but also computationally efficient and scalable.

A key approach to mitigating computational costs is the use of emulators, such as Gaussian processes (GPs), which approximate expensive simulations while retaining predictive accuracy and providing robust UQ. Emulators enable faster inference in many-query problems like calibration, but their effectiveness depends on the choice of training data. Selecting informative simulation runs to build the emulator is critical, as inefficient sampling can lead to poor calibration performance and unnecessary computational expense.

This paper examines Bayesian calibration of expensive models using emulators, focusing on different data acquisition strategies. We compare four key approaches: Bayesian Optimal Experimental Design (BOED) [33, 5, 20] and its goal-oriented extension (GBOED) [60, 1, 2]), Calibrate Emulate Sample (CES) [7], and History Matching (HM) [9]. Among these, optimal experimental design (OED) methods like BOED have been widely applied to guide physical experiments and sensor placement [58, 48, 18], but their potential for selecting computer simulations in emulator-based calibration remains underexplored.

Our contributions are twofold. First, we introduce a novel goal-oriented BOED (GBOED) algorithm that extends standard BOED to optimize information gain about the posterior distribution, making it more effective for calibration tasks. Second, we provide a comprehensive comparative study of BOED, GBOED, CES, and HM, evaluating their trade-offs in computational cost, implementation complexity, and UQ performance. Our results offer new insights into the practical merits and limitations of BOED-based methods for calibration and contribute to the broader discussion of how best to integrate experimental design principles into Bayesian inference for expensive models.

## 1.1 Background and motivation

We are specifically interested in exploring these methods for accelerating the calibration of computationally expensive climate models, because this type of calibration task exemplifies the challenges of combining UQ with real-world applications. Climate models play a crucial role in enhancing our understanding of climatological phenomena, allowing us to monitor current and past climatic conditions and forecast future trends [52, 25, 46]. Over time, these models have been refined to incorporate a multitude of intricate components, including wind patterns, atmospheric conditions, and more [51, 14, 30]. The utility of climate models,

however, hinges on parameter settings that influence complex, interconnected processes across the atmosphere, oceans, and land surfaces. Calibrating physical and empirical parameters with UQ is critical for obtaining realistic model simulations and reducing climate model uncertainty. Calibration is especially challenging for climate models due to their complexity, computational demands, and the chaotic nature of the underlying systems, which amplifies uncertainty and hinders reliable parameter estimation.

Similar to other domains that depend on expensive physics models, calibration of climate models has historically been accomplished by manually setting parameters such that model output best matches observations, a task that requires the expertise of climate scientists [49]. This approach may introduce bias, ignore variability and uncertainty in model outputs [49], and fail to adequately capture parameter interactions. Recent research in climate calibration has sought to automate the calibration process. For instance, [59] proposes a scalable approach in which an emulator is trained on a limited number (250) of climate model simulations. The trained emulator is then used within an optimization procedure to determine optimal parameter values based on observations. The method proposed by [59] falls into a broad category of approaches called Bayesian calibration, in which parameter estimates and their uncertainty are rigorously quantified via a probability distribution, rather than a fixed value. Since the seminal paper that introduced the formalism of Bayesian calibration of computational models in 2001 [26], interest in this method has grown steadily in several fields [53], including biology [23], engineering [15, 17], physics [34] and climate science [24, 11, 6, 56, 27, 59, 50].

Efficient emulators are an important component of a Bayesian calibration framework, allowing it to scale to larger parameter spaces. In contrast to expensive models, emulators can be evaluated efficiently thousands to millions of times, which is necessary for Markov Chain Monte Carlo (MCMC) sampling typically involved in Bayesian calibration. A critical challenge in Bayesian calibration is selecting the limited set of model runs needed to train the emulator while maximizing its accuracy for calibration tasks. Traditional sampling strategies, such as Monte Carlo sampling and space-filling designs like Quasi Monte Carlo [42] and Latin hypercube sampling [38] improve efficiency compared to dense grids but are not specifically tailored to the downstream goal of calibration.

Methods such as History Matching (HM) [57] and Calibrate, Emulate, Sample (CES) [7] aim to address this gap by focusing sampling on regions of the parameter space relevant to calibration. HM iteratively refines the parameter space by eliminating implausible regions, dramatically reducing computational costs [57]. It does not provide UQ on its own, although it can be combined with MCMC sampling to produce a posterior distribution over calibration parameters, which is the approach we take. CES incorporates information from the calibration problem into its sampling strategies. CES is unique in that it combines Kalman filtering, GP emulation, and MCMC sampling to iteratively refine the posterior, providing systematic UQ at each stage [7].

Leveraging the formalism of Bayesian theory, BOED and GBOED extend these ideas by framing the design of model evaluations as an optimization problem. Within its standard formulation, BOED selects simulation designs that maximize the expected information gained about the emulator, leveraging the probabilistic nature of GPs to guide decisions. GBOED refines this approach further by focusing on regions of the parameter space that directly reduce uncertainty in the posterior distribution, making it particularly well-suited for calibration

tasks. In essence, GBOED works by resolving intermediate calibration problems, leveraging the surrogate and its associated uncertainty. While BOED has been shown to achieve reliable calibration results for climate models with fewer model evaluations [12], the use of GBOED for calibration-specific tasks has not been explored in the literature.

This paper is structured as follows: first, we review GP emulators (Section 2.1) and then provide an overview of the main methods (BOED, GBOED, CES, and HM) (Sections 2.2-2.4). Next, we describe the experimental setup (Section 3.2), validation (Section 3.1), and the model on which we test our methods (Section 4.2.1). Finally, we provide results regarding performance of all the methods (Section 4.2.2) and concluding remarks (Section 5).

## 2 Methods

In this study, we assume we have access to simulations from a climate model  $\mathcal{G}$ , which is typically very computationally expensive. Due to the computational intensity of  $\mathcal{G}$  we seek to approximate it with a cheap emulator whenever we need to evaluate it many times, e.g. for model calibration. Typically the emulator does not capture the full output of  $\mathcal{G}$ , e.g. a very high dimensional spatiotemporal dataset, but only a reduced dimensional output comprised of important quantities of interest for solving the calibration problem. Since output quantities of interest from  $\mathcal{G}$  are usually  $p > 1$  dimensional, two types of emulators may be considered. If outputs can be reasonably considered independent of one another,  $p$  individual emulators can be used for modeling each component output. Alternatively, a multi-output emulator can be used to model correlation among the  $p$  component outputs. Here, we consider independent GP emulators for each output dimension for reduced computational burden. Gaussian processes (GPs) are a natural choice for emulation due to their well-calibrated uncertainty quantification (UQ), flexibility, and analytical tractability, making them particularly well-suited for Bayesian calibration [55]. However, a wide variety of emulators have been used in the literature, including deep neural networks [3, 36], polynomial chaos expansions [39], and other machine learning methods [54].

### 2.1 Bayesian Calibration with GP emulators

Bayesian calibration provides a probabilistic framework for inferring unknown model parameters and incorporating both prior knowledge and observational data. Given observations  $y_{obs}$  and a computational model  $\mathcal{G}$  that maps parameters  $\theta$  to model output, we assume the relationship  $y_{obs} = \mathcal{G}(\theta) + \eta$  where  $\eta$  accounts for observational noise and model discrepancy. The goal is to estimate the posterior distribution of  $\theta$  given  $y_{obs}$ , which follows from Bayes' Theorem:

$$p(\theta | y_{obs}) = \frac{p(y_{obs} | \theta)p(\theta)}{p(y_{obs})}. \quad (1)$$

When we assume that the likelihood,  $p(y_{obs} | \theta)$ , is Gaussian, then

$$p(y_{obs} | \theta) = \frac{1}{(2\pi)^{p/2}|\Gamma_{obs}|^{1/2}} \exp\left(-\frac{1}{2}(y_{obs} - \mathcal{G}(\theta))^T \Gamma_{obs}^{-1}(y_{obs} - \mathcal{G}(\theta))\right), \quad (2)$$

where  $\Gamma_{obs}$  reflects uncertainty among observations and  $p$  is the output dimension. In principle, we can find the posterior using MCMC to generate samples from the distribution, but this would be computationally prohibitive, because it would require evaluating  $\mathcal{G}$  thousands of times. Instead, we consider a GP emulator that approximates the mapping from  $\theta$  to  $\mathcal{G}(\theta)$ . While  $\theta$  denotes the model parameters to be calibrated, we use  $\mathbf{X} = \{x_1^\top, x_2^\top, \dots, x_m^\top\}$  to represent inputs to the GP emulator in order to distinguish calibrating the model from training the emulator. These inputs correspond to sampled locations in the parameter space, which may include  $\theta$ .

Here, we provide a brief review of GPs for surrogate modeling. For more details see [55] or [22]. Consider the expensive computer model  $\mathcal{G}$  represented as a function  $f : \mathbb{R}^d \rightarrow \mathbb{R}^p$  that maps inputs to outputs, whose pairs over  $n$  simulations comprise data  $D = (\mathbf{X}, \mathcal{G}(\mathbf{X}))$ , where inputs (model parameters) are  $\mathbf{X} = \{x_1^\top, x_2^\top, \dots, x_m^\top\} \in \mathbb{R}^{m \times d}$  and  $\mathcal{G}(\mathbf{X}) = \{\mathcal{G}(x_1)^\top, \mathcal{G}(x_2)^\top, \dots, \mathcal{G}(x_m)^\top\} \in \mathbb{R}^{m \times p}$  are corresponding model outputs. Since we use independent GP emulators for each output dimension, we consider modeling the individual components  $\mathcal{G}_i(\mathbf{X}), i = 1 \dots p$ . For notational simplicity, let  $\mathbf{Y}$  represent a single component output of  $\mathcal{G}(\mathbf{X})$ . Assuming a zero-mean GP prior for each component output of  $f$  implies that  $\mathbf{Y}$  follows a multivariate normal distribution (MVN) with a mean of zero and a covariance  $\Gamma_{GP}$  that is determined by inverse distances between inputs  $\mathbf{X}$ :

$$\mathbf{Y} \sim \mathcal{N}(\mathbf{0}, \Gamma_{GP}(\mathbf{X})) \quad \text{where, e.g.,} \quad \Gamma_{GP}^{k\ell} = \tau^2(k(q(x_k, x_\ell)) + g\mathbb{I}_{\{k=\ell\}}), \quad (3)$$

where a kernel,  $k(\cdot)$ , transforms distances, and  $q(\cdot, \cdot)$  calculates a scaled squared Euclidean distance:

$$q(x_i, x_j) = \left( \sum_{\ell=1}^p \frac{\|x_{i,\ell} - x_{j,\ell}\|^2}{\gamma_\ell} \right)^{1/2}.$$

The  $\boldsymbol{\gamma} = (\gamma_1, \gamma_2, \dots, \gamma_d)$  are *lengthscale* or *range* parameters, where  $1/\gamma_\ell$  determines the ‘‘relevance’’ of the  $x_\ell$  input,  $\tau^2$  governs the magnitude of the response, and the nugget  $g$  divides the magnitude between signal ( $\tau^2$ ) and noise ( $\tau^2 g$ ). The GP model in Eq. (3) for  $\mathbf{Y}$  gives rise to a MVN likelihood:

$$L(\boldsymbol{\phi}; D) \propto |\Gamma_{GP}|^{-1/2} \exp\left(-\frac{1}{2} \mathbf{Y}^\top \Gamma_{GP}^{-1} \mathbf{Y}\right). \quad (4)$$

We express the framework in Eq. (3) as  $\mathcal{GP}(D)$ , which is defined by a choice of  $k(\cdot)$ ,  $q(\cdot)$ , and hyperparameters  $\boldsymbol{\phi} = (\boldsymbol{\gamma}, \tau^2, g)$ . Hyperparameter estimates  $\hat{\boldsymbol{\phi}}$  are learned from the data,  $D$ , via the likelihood in 4 via maximum a posteriori (MAP) estimation. Typically, the predictive mean from  $\mathcal{GP}(D)$  at new locations  $\mathcal{X}$  is of primary interest. Ultimately,  $\mathcal{GP}(D)$  can be used to obtain the posterior predictive distribution  $\mathbf{Y}(\mathcal{X})|D$ , which is conditional on estimated hyperparameter values. The resulting posterior predictive distribution, also an MVN, can be obtained through the MVN conditioning equations:  $\mathbf{Y}(\mathcal{X})|D \sim \mathcal{N}(\boldsymbol{\mu}_{GP}(\mathcal{X}), \Gamma_{GP}(\mathcal{X}))$ . Therefore, incorporating the GP predictive mean and variance into Eq. (2) provides the following likelihood for the emulator-based calibration problem:

$$p(y_{obs} | \theta, \mathcal{GP}(D)) = \frac{e^{-\frac{1}{2}(y_{obs} - \boldsymbol{\mu}_{GP}(\theta))^T (\Gamma_{GP}(\theta) + \Gamma_{obs})^{-1} (y_{obs} - \boldsymbol{\mu}_{GP}(\theta))}}{(2\pi)^{n/2} |\Gamma_{GP}(\theta) + \Gamma_{obs}|^{1/2}}. \quad (5)$$

Because obtaining predictions from the GP emulator at any new inputs is cheap, MCMC can be used to perform Bayesian calibration via Eq. (5) while incorporating the model discrepancy due to the use of a GP emulator. The key challenge is judiciously choosing simulation training data  $D$  to produce the most accurate and efficient emulator to be used in the calibration problem.

## 2.2 Bayesian Optimal Experimental Design

Optimal Experimental Design (OED) focuses on identifying and optimizing data collection strategies to maximize the amount of information gained from experiments. In this context, information gain typically refers to changes in beliefs toward a reduction in the uncertainty of model parameters. Within the Bayesian paradigm, BOED seeks to collect data that maximizes the Expected Information Gain (EIG), which quantifies how much the posterior distribution reduces uncertainty relative to the prior, measured using Kullback-Leibler (KL) divergence. BOED is a theoretically rigorous approach but can be computationally intensive and sensitive to assumptions [5]. In this context, we emphasize that the data being collected are not direct observations ( $y_{obs}$ ) but rather data arising from simulations used to fit an emulator.

Ideally, we formulate the BOED problem to maximize the EIG about the model parameters we wish to infer. Suppose we have initial data  $D = (\mathbf{X}_{init}, \mathbf{Y}_{init})$  and that a zero-mean GP is fit to  $D$ , e.g. ( $\mathcal{GP}(D)$ ). Let  $\mathbf{X}$  represent an initial design of inputs chosen via a space-filling method such as Latin Hypercube Sampling (LHS) or Quasi Monte Carlo sampling. These inputs are selected to provide a representative coverage of the parameter space and to initialize the GP emulator. We can measure how much information we expect to gain about  $\theta$  when training on  $D$  by computing the EIG:

$$\begin{aligned} EIG(\mathbf{X}) &= \int p(\mathbf{Y}|\mathbf{X}) \int p(\theta|y_{obs}, \mathcal{GP}(D)) \log \frac{p(\theta|y_{obs}, \mathcal{GP}(D))}{p(\theta)} d\theta d\mathbf{Y} \\ &= \int p(\mathbf{Y}|\mathbf{X}) \int p(\theta|y_{obs}, \mathcal{GP}(D)) \log \frac{p(y_{obs}|\theta, \mathcal{GP}(D))}{p(y_{obs}|\mathcal{GP}(D))} d\theta d\mathbf{Y} \end{aligned} \quad (6)$$

In Eq. (6),  $\mathbf{Y}|\mathbf{X}$  are realizations from the GP prior. In addition,  $p(\theta|y_{obs}, \mathcal{GP}(D))$  is the posterior distribution of parameters  $\theta$ ,  $p(\theta)$  is the prior distribution on  $\theta$ , and  $p(y_{obs}|\theta, \mathcal{GP}(D))$  is the likelihood. We wish to choose the design  $\mathbf{X}^*$  that maximizes the  $EIG$ ; that is, given bounds on the input space ( $\Xi$ ), we wish to find  $\mathbf{X}^* = \arg \max_{\mathbf{X} \in \Xi} EIG(\mathbf{X})$ . The expression in 6 represents the “idealized” OED problem and is rarely implemented in practice. Computing the EIG in the idealized OED problem is challenging, because for each candidate design  $\mathbf{X}$ , we must sample realizations  $\mathbf{Y}$  from the GP prior predictive distribution, solve the calibration problem to obtain  $p(\theta|y_{obs}, \mathcal{GP}(D))$ , and estimate the KL divergence or the marginal model evidence  $p(y_{obs}|\mathcal{GP}(D))$ .

To solve the idealized OED problem in Eq. (6), a sequential approach may be taken, where we iteratively optimize the EIG to determine an initial design  $\mathbf{X}_0$ , run simulations, and then conditionally optimize additional simulations. For the updated training dataset, we include new points  $\mathbf{X}_1 = \mathbf{X}_0 \cup \mathbf{X}_{new}$ , where  $\mathbf{X}_{new}$  represents newly selected inputs. This iterative

process ensures that simulation samples are strategically placed to improve calibration performance of the emulator, rather than being driven by uninformed priors. Without this sequential refinement, samples are less effective, as they rely solely on prior information that may be uninformative. However, sequential refinement is computationally expensive, as it requires repeatedly solving the calibration problem and updating the emulator. In what follows, we emphasize two practical experimental design strategies: standard BOED, which maximizes EIG about the emulator, and goal-oriented BOED (GBOED), which prioritizes information gain about the inferred parameters. For completeness, we describe the “idealized” BOED formulation as a conceptual gold standard (though computationally infeasible for real-world problems) and compare it against BOED and GBOED in SM4.

When applying BOED to maximize the EIG for a GP emulator, we aim to maximize information gain about GP outputs, which is directly tractable. Assuming the specification of a GP prior for  $\mathbf{Y}$ , consider an extended candidate set of inputs  $\mathbf{X}'$  where  $\mathbf{X} \subset \mathbf{X}'$  and for which  $\mathbf{Y}' \sim \text{MVN}(\mathbf{0}, \mathbf{K}(\mathbf{X}'))$  reflects the GP prior evaluated at  $\mathbf{X}'$ . The posterior predictive distribution of  $\mathbf{Y}'$  at inputs  $\mathbf{X}'$  given training data  $D = (\mathbf{X}, \mathbf{Y})$  is denoted as  $\mathbf{Y}'|\mathbf{X}', \mathcal{GP}(D)$ . In the standard BOED approach, the EIG is defined as Eq. (7):

$$EIG(\mathbf{X}) = \int p(\mathbf{Y}|\mathbf{X}) \int p(\mathbf{Y}'|\mathbf{X}', \mathcal{GP}(\mathbf{X}, \mathbf{Y})) \log \frac{p(\mathbf{Y}'|\mathbf{X}', \mathcal{GP}(\mathbf{X}, \mathbf{Y}))}{p(\mathbf{Y}'|\mathbf{X}')} dx d\mathbf{Y}. \quad (7)$$

This expression quantifies how much we expect the GP posterior to differ from the GP prior at candidate locations  $\mathbf{X}'$ , on average. Let the (zero-mean) GP prior have covariance matrix  $\mathbf{K}_{\mathbf{X}', \mathbf{X}'}$ , and let the posterior predictive variance at  $\mathbf{X}'$  after observing data  $\mathcal{D} = (\mathbf{X}, \mathbf{Y})$  be denoted by  $\mathbf{\Sigma}'$ . Then, the EIG in (7) can be expressed in closed form as the expected KL divergence (over  $\mathbf{Y}$ ) between two multivariate Gaussian distributions (Eq. 8) (see proof in SM5):

$$EIG(\mathbf{X}) = \frac{1}{2} \log \left( \frac{\det(\mathbf{K}_{\mathbf{X}', \mathbf{X}'})}{\det(\mathbf{\Sigma}')} \right), \quad (8)$$

$$\mathbf{\Sigma}' = \mathbf{K}_{\mathbf{X}', \mathbf{X}'} - \mathbf{K}_{\mathbf{X}', \mathbf{X}} \mathbf{K}_{\mathbf{X}, \mathbf{X}}^{-1} \mathbf{K}_{\mathbf{X}, \mathbf{X}'}$$

The algorithm for standard BOED is given in Algorithm 2.1.

In practice, not all GP outputs are equally relevant to calibration. To further improve efficiency, we introduce a goal-oriented BOED (GBOED) strategy, which focuses on predicting values most relevant to the calibration posterior. Instead of choosing a generic set of test inputs  $\mathbf{X}'$ , GBOED utilizes test locations drawn from the current posterior of  $\theta$ , i.e.,  $\mathbf{X}' \sim p(\theta|y_{obs}, \mathcal{GP}(D))$ . The GP is then optimized to gain information only about predictions at those points likely under the posterior, thereby aligning the training design more closely with the calibration task (see Algorithm 2.2). While BOED and GBOED differ in the choice of  $\mathbf{X}'$ , we note that if  $\mathbf{X}'$  becomes dense in the input space (i.e., fully explores the emulator domain), then GBOED recovers standard BOED. We prove this in the finite case (see SM1). This theoretical equivalence justifies GBOED as a goal-oriented simplification of BOED that prioritizes the most relevant parts of the input space for calibration. For the interested reader, SM4 shows the differences in BOED, GBOED and idealized OED when applied to a toy calibration problem.

---

**Algorithm 1** Standard Bayesian Optimal Experimental Design (BOED)

---

**Input:** Bounds for input space  $\Xi$ , initial number of samples  $n_0$ , simulation budget  $N$ , GP emulator  $\mathcal{GP}$

**Output:** Samples from calibrated posterior distribution  $p(\theta \mid y_{\text{obs}}, \mathcal{GP}(D))$

- 1: Select an initial set of  $n_0$  input samples  $\mathbf{X}_{\text{init}}$  from  $\Xi$ .
  - 2: Run the simulation  $\mathcal{G}$  for each input in  $\mathbf{X}_{\text{init}}$  to generate outputs  $\mathbf{Y}_{\text{init}}$ .
  - 3: Train  $\mathcal{GP}$  using the dataset  $D = \{\mathbf{X}_{\text{init}}, \mathbf{Y}_{\text{init}}\}$ .
  - 4: **for**  $i = 1$  to  $N - n_0$  **do** ▷ Remaining simulation budget
  - 5:     Initialize a candidate input  $\mathbf{x}_{\text{cand}}$  within  $\Xi$ .
  - 6:     **for** iteration = 1 to desired optimization steps **do** ▷ Optimize EIG
  - 7:         Compute the Expected Information Gain (EIG) for  $\mathbf{x}_{\text{cand}}$  using Eq. (8).
  - 8:         Update  $\mathbf{x}_{\text{cand}}$  to improve the EIG.
  - 9:     **end for**
  - 10:     Select the optimized input  $\mathbf{x}^*$  with the highest EIG.
  - 11:     Run the simulation  $\mathcal{G}$  at  $\mathbf{x}^*$  to obtain its output  $y^*$ .
  - 12:     Add  $\{\mathbf{x}^*, y^*\}$  to the dataset  $D$ .
  - 13:     Refit  $\mathcal{GP}$  using the updated dataset  $D$ .
  - 14: **end for**
  - 15: Solve the Bayesian calibration problem using MCMC with the GP emulator.
-

---

**Algorithm 2** Goal-Oriented Bayesian Optimal Experimental Design (GBOED)

---

**Input:** Bounds for input space  $\Xi$ , initial number of samples  $n_0$ , simulation budget  $N$ , GP emulator  $\mathcal{GP}$

**Output:** Samples from the posterior distribution  $p(\theta \mid y_{\text{obs}}, \mathcal{GP}(D))$

- 1: Select an initial set of  $n_0$  input samples  $\mathbf{X}_{\text{init}}$  from  $\Xi$ .
- 2: Run the simulation  $\mathcal{G}$  for each input in  $\mathbf{X}_{\text{init}}$  to generate outputs  $\mathbf{Y}_{\text{init}}$ .
- 3: Train  $\mathcal{GP}$  using the dataset  $D = \{\mathbf{X}_{\text{init}}, \mathbf{Y}_{\text{init}}\}$ .
- 4: **for**  $i = 1$  to  $N - n_0$  **do** ▷ Remaining simulation budget
- 5:     Solve the calibration problem using MCMC with the current surrogate model:

$$\mathbf{X}' \sim p(\theta \mid y_{\text{obs}}, \mathcal{GP}(D))$$

- 6:     Initialize a candidate input  $\mathbf{x}_{\text{cand}}$  within  $\Xi$ .
- 7:     **for** iteration = 1 to desired optimization steps **do** ▷ Optimize EIG
- 8:         Compute the Expected Information Gain (EIG) for  $\mathbf{x}_{\text{cand}}$  with respect to the predictions at  $\mathbf{X}'$  via Eq. (8).
- 9:         Update  $\mathbf{x}_{\text{cand}}$  to maximize  $EIG(\mathbf{x}_{\text{cand}})$ .
- 10:     **end for**
- 11:     Select the optimized input  $\mathbf{x}^*$  with the highest EIG.
- 12:     Run the simulation  $\mathcal{G}$  at  $\mathbf{x}^*$  to obtain its output  $y^*$ .
- 13:     Add  $\{\mathbf{x}^*, y^*\}$  to the dataset  $D$ .
- 14:     Refit  $\mathcal{GP}$  using the updated dataset  $D$ .
- 15: **end for**
- 16: Solve the final Bayesian calibration problem using MCMC using the GP emulator to obtain posterior samples:

$$\mathbf{X}' \sim p(\theta \mid y_{\text{obs}}, \mathcal{GP}(D)).$$

---

## 2.3 Calibrate, emulate, sample

Calibrate, Emulate, Sample (CES) [7] is a sequential framework designed to efficiently tackle Bayesian calibration problems for computationally expensive models. By combining ensemble-based calibration techniques, GP emulators, and MCMC sampling, CES provides a scalable approach to parameter estimation while ensuring robust UQ. It is a practical choice for large-scale or high-dimensional problems and its general framework make it suitable for a variety of applications.

At a high level, CES starts with a calibration phase, in which ensemble Kalman filter techniques such as Ensemble Kalman Inversion (EKI) [28] or Ensemble Kalman Sampling (EKS) [19], are used to obtain an initial posterior distribution of parameters based on a limited number of model evaluations. The next phase, Emulate, involves training an efficient GP emulator on parameter samples (inputs) and model outputs(s) obtained during the Calibration phase. This emulator is a computationally cheap surrogate for  $\mathcal{G}$ .

In the final phase, Sample, MCMC sampling is utilized to further refine the posterior of  $\theta$ . Employing MCMC in conjunction with the GP emulator enables the drawing of samples from the approximate posterior distribution, thereby ensuring robust UQ. The computational

efficiency and inherent smoothness of GP emulators allows for the use of MCMC, which may be prohibitive for expensive  $\mathcal{G}$ .

We implement CES following methods specified in [7]. We use EKS for the calibration phase, since EKS (unlike EKI) does not suffer from the collapse of the posterior distribution to a point mass [19]. EKS is used only for a limited number of iterations to reduce the computational burden, so the subsequent steps of CES (Emulation and Sampling) are usually necessary to obtain reliable UQ and refinement of the posterior distribution of  $\theta$ .

## 2.4 History Matching

HM is a statistical methodology that leverages observed data to refine model parameters by ruling out “implausible” parameter values based on how well they match the observations [56]. By iteratively updating parameter configurations, HM effectively narrows the range of plausible values, thereby reducing the computational costs associated with the expensive model simulations. History matching is well-represented in the field of climate science and has been used extensively for climate model calibration [8, 57, 56, 16, 47, 31].

HM is an iterative process, conducted in “waves,” where regions of the parameter space deemed implausible are progressively eliminated. Implausible regions are parameter configurations that are highly unlikely to produce model outputs resembling the observed data. The remaining parameter space, known as the “Not-Ruled-Out-Yet” (NROY) space, becomes increasingly refined through successive waves. This iterative narrowing continues until a user-defined stopping criterion is met.

The first wave is initiated with sampling a limited number of parameter configurations from the entire parameter space. These configurations are used to run the computationally expensive model, and the inputs combined with resulting model outputs form a training dataset to fit a GP emulator. Given the high computational cost of running the model, it is essential to carefully choose a small but representative set of samples. These samples are typically drawn using methods like Optimal Experimental Design (OED) or Latin Hypercube Sampling (LHS) [38]. In our work, we employ LHS because it is straightforward to implement and computationally efficient. For high-dimensional problems, taking advantage of OED for sampling would be better than LHS, because the initial set would be information rich.

After fitting the GP emulator, we use it to partition the parameter space into plausible and implausible regions, the classification of which is based on an implausibility metric that measures the discrepancy between the model outputs and observed data:

$$I(\theta) = \frac{||\mathcal{GP}(\theta) - y_{obs}||}{\sqrt{Var(y_{obs}) + Var(\mathcal{GP}(\theta))}}. \quad (9)$$

In Eq.(9),  $Var(y_{obs})$  represents the variance of the observations, while  $Var(\mathcal{GP}(\theta))$  reflects the uncertainty estimates from the GP model at each input. The metric evaluates how well a parameter configuration reproduces the observed data, accounting for both observational and emulator uncertainties.

We evaluate Eq.(9) at one million random points in the parameter space, which ensures that enough points remain for subsequent waves after each wave of history matching. Regions of the parameter space where the implausibility metric is above a certain threshold are

discarded, as those parameter configurations are unlikely to have generated the observed data. A threshold of three suffices due to the “three-sigma” rule defined in [44], which states that for any continuous, unimodal distribution, 95% of its probability will lie within  $\pm 3\sigma$  of the mode regardless of the distribution’s asymmetry, skewness, or heavy tails (see Algorithm 2.3).

Subsequent waves refine the NROY space further. For each wave, new training samples are drawn from within the current NROY space, the expensive model is run, and the emulator is updated. Sampling from the NROY space is challenging because uniform sampling is infeasible when the space becomes fragmented due to eliminated “clusters of inputs”. Instead, we sample uniformly from the remaining points already identified as part of the NROY space. The HM process continues until a stopping criterion is met. This could be based on computational constraints or when the NROY space becomes too small to warrant further refinement. In our implementation, we use a fixed threshold of three for the implausibility metric in all waves and rely on the available computational budget to determine when to stop. To automate the HM process, [10] proposes a semi-automated approach using sequential MCMC, which eliminates the need for user-specified parameters like implausibility thresholds. Instead, we adhere to a simpler framework with fixed thresholds and computational constraints guiding our stopping criteria. Importantly, while the HM algorithm technically ends when the stopping criteria is reached, we apply an extra MCMC step, based on the GP emulator fitted to samples in the final wave. Unlike traditional HM, the final MCMC step allows us to construct a posterior distribution for calibration parameters.

---

**Algorithm 3** History Matching Algorithm

---

- 1: **Input:** Initial set of parameter sample bounds  $bounds$ , expensive model  $\mathcal{G}$ , observations  $y_{obs}$
  - 2: **Output:** Refined Not ruled out yet (NROY) space
  - 3: Generate uniform samples of the parameters within the bounds,  $\theta_{bounds}$ .
  - 4: Generate corresponding outputs  $\mathcal{G}(\theta_{bounds})$  for  $\theta_{bounds}$ .
  - 5: Train GP emulator using samples from the simulator,  $(\theta_{bounds}, \mathcal{G}(\theta_{bounds}))$
  - 6: **for** each wave of history matching **do**
  - 7:     **for** each column of outputs **do**
  - 8:         Compute implausibility metric  $I(\theta)$  for each sample using Eq. (9).
  - 9:         Remove regions of parameter space with  $I(\theta) > 3$
  - 10:     **end for**
  - 11:     Take the intersection of the NROY space across all outputs
  - 12:     Sample new points uniformly from the refined NROY space
  - 13:     Retrain the GP emulator with the new samples
  - 14: **end for**
  - 15: **End** when stopping criterion (e.g., computational budget) is met
-

### 3 Experimental setup

We use the Lorenz '96 multiscale system described in [35] (Eq. 10) to test our methods. The Lorenz '96 system is a simplified mathematical model that is often used to study the behavior of chaotic systems such as climate [32, 41, 40, 43]. The system consists of a set of ordinary differential equations that describe the evolution of a large number of interacting variables. In this system, there are  $K$  large-scale variables ( $X_k$ ) and  $JK$  small-scale variables ( $Y_{j,k}$ ). The  $X$  and  $Y$  variables interact with each other, but there is also coupling between them, as shown in Eq. (10).

$$\begin{aligned}\frac{dX_k}{dt} &= -X_{k-1}(X_{k-2} - X_{k+1}) - X_k - \frac{hc}{b} \sum_{j=1}^J Y_{j,k} + F \\ \frac{dY_{j,k}}{dt} &= -cbY_{j+1,k}(Y_{j+1,k} - Y_{j-1,k}) - cY_{j,k} + \frac{hc}{b} X_k.\end{aligned}\tag{10}$$

The large- and small-scale variables are periodic over  $J$  and  $K$ , i.e.,  $X_{k-K}, X_{k+K} = X_k$ , and  $Y_{j,k-K}, Y_{j,k+K} = Y_{j,K}$  and  $Y_{j-J,k} = Y_{j,k-1}$ , and  $Y_{j+J,k} = Y_{j,k+1}$ . The parameters of the system,  $\theta = (h, F, c, b)$ , control the degree of forcing, coupling, and amplitude of the system.

We perform Bayesian inversion for  $\theta$  based on data averaged across the  $K$  locations and over time windows of length  $T = 100$  for all methods. We consider the following observables arising from the  $k$ -indexed operator  $\varphi_k : \mathbb{R} \times \mathbb{R}^J \rightarrow \mathbb{R}^5$  as defined in [7]:  $\phi_k(Z) = \phi(X_k, Y_{1,k}, \dots, Y_{J,k}) = (X_k, \bar{Y}_k, X_k^2, X_k \bar{Y}_k, \bar{Y}_k^2)$ , where  $Z$  characterizes the current state of the system.

Generally, it can be assumed that the observations arising from this system can be expressed as a forward operator  $\mathcal{G}(\cdot)$  acting on input parameters  $\theta$  plus noise:

$$y = \mathcal{G}(\theta) + \eta,\tag{11}$$

where  $\eta \sim N(0, \Gamma_y(\theta))$  and  $\Gamma_y(\theta) = T^{-1}\Sigma(\theta)$ . Typically,  $\Gamma_y(\theta)$ , which captures variability due to initial conditions, must be approximated by  $\Gamma_{obs}$ . To obtain  $\Gamma_{obs}$  we simulate the Lorenz '96 system for a  $\tau = 40,000$  time steps and calculate the covariance over windows of  $T = 100$ , in accordance with [7]. The forward operator is then defined as:

$$\mathcal{G}(\theta) = \frac{1}{T} \int_0^T \left( \frac{1}{K} \sum_{k=1}^K \phi_k(Z(s)) \right) ds.$$

#### 3.1 Performance metrics

We consider two validation metrics, absolute error (AE) and proper (log) score (Eq. 25 in [21]), which balances accuracy in point estimates as well as UQ. In the equations for AE and score below,  $\hat{\mu}$  and  $\hat{\sigma}$  are the estimated means and standard deviations for components (e.g.  $h, F, c, b$ ) of  $\theta$ , and  $y$  represents the corresponding true value. Score and AE are calculated as follows:

$$\begin{aligned}\text{AE}(y, \hat{\mu}) &= |y - \hat{\mu}|, \\ \text{score}(y, \hat{\mu}, \hat{\sigma}) &= -\log(\hat{\sigma}^2) - (y - \hat{\mu})^\top \frac{1}{\hat{\sigma}^2} (y - \hat{\mu}).\end{aligned}$$

Smaller AEs and larger scores are preferred. Prior to calculating validation metrics, values for the parameter  $\log c$  of the Lorenz '96 system were exponentiated. Because all methods provide a posterior distribution for components of  $\theta$ , we use the empirical means and standard deviations as point estimates for each component of  $\theta$  in computing validation metrics.

## 3.2 Implementation details

To assess how the performance of methods changed with increasing model evaluations, we performed calibration twice with each method, using relatively few (200) and more (1000-5400) model evaluations. We chose 200 model evaluations based on methodology in [59], and 1000 represents a reasonable upper bound for the number of simulations that would be practically feasible with an expensive climate model [11, 13]. To obtain the final posterior distribution for  $\theta$  for all methods, we use GP emulators, along with corresponding  $\phi_k(Z)$  and  $\Gamma_{obs}$  to perform MCMC sampling. Recall that because the observables are five-dimensional, five independent GPs were fitted. We use the same prior specification for GP lengthscales as specified in [7] for all methods for consistency. MCMC sampling was conducted via Sequential Tempered Markov Chain Monte Carlo (ST-MCMC) [4], which is a highly effective Sequential Monte Carlo (SMC) sampler due to its efficient parallelism while retaining sampling robustness due to its adaptivity and monitoring of sample population statistics instead of individual chain statistics. We found that 8192 ST-MCMC parallel samples resulted in a comprehensive exploration of the posterior for all methods. See [4] for more details on ST-MCMC sampling.

### 3.2.1 CES and EKS

For performing Bayesian inversion on the Lorenz '96 system (Eq. 10) via CES, EKS was run for 54 iterations with 100 ensemble members (5400 model evaluations), in accordance with [7]. We also ran EKS with only 10 iterations and 20 ensemble members (200 model evaluations). For the case of 5400 model evaluations, only iterations 1, 6, 12,  $\dots$ , 54 were saved for subsequent GP fitting, as suggested in [7]. Doing so reduces the total number of data required to fit GPs, decreasing computation time while retaining the spread of the samples over the total number of EKS iterations.

### 3.2.2 BOED and GBOED

For both BOED and GBOED with 200 or 1000 total evaluations, the initial GP model was trained using 64 Quasi Monte Carlo samples from the Sobol Sequence to ensure space-filling coverage of the input domain. These initial samples guided subsequent greedy OED choices. The remaining samples were selected using the optimization procedures outlined in Algorithms 2.1 and 2.2, with ST-MCMC employed for the intermediate sampling required by GBOED.

### 3.2.3 HM

For HM, we used both 40 model evaluations across five waves (200 total evaluations) and 200 model evaluations across 5 waves (1000 total evaluations). To obtain the final posterior distribution of the parameters, we use the final trained GP emulators to perform ST-MCMC sampling.

For reporting results, all methods are named using the method name (i.e., BOED, GBOED, CES, HM) followed by a suffix indicating the number of model evaluations. For example, CES5400 refers to the CES method where  $\mathcal{G}(\cdot)$  is evaluated 5400 times.

## 4 Experiments

In this section, we describe three experiments pertaining to calibration of the Lorenz '96 multiscale system using the main methods CES, HM, BOED, and GBOED. We begin with examining the marginal posterior distributions of  $h$ ,  $F$ ,  $c$  and  $b$ . Next, we conduct a convergence analysis of all methods over increasing model evaluations, and finally, we conduct an in-depth performance assessment comparing accuracy and UQ of all methods.

First, we show the posterior distribution resulting from all methods for  $\theta = (1, 10, 10, 10)$ . Posterior distributions for  $h$ ,  $F$ ,  $c$  and  $b$  for the case of fewer (200) and more (1000-5400) model evaluations resulting from the main methods CES, HM, BOED, and GBOED are shown in the left and right panels, respectively, of Figure 1 (recall that CES was run with 5400 model evaluations following methods in [7]). Due to the nonlinear and chaotic nature of the Lorenz '96 system and correlation among parameters, the resulting posterior distributions are not expected to be Gaussian. Indeed, our MCMC samples often exhibit skewness and heavy tails.

While posterior distributions for each of the four parameters appear similar across methods, there are some differences. Notably, the ranges for parameter  $c$  for CES, BOED, and GBOED are much wider (0-50) compared to that of HM (0-20), and this is consistent regardless of the number of model evaluations used. Posteriors for parameter  $b$  tend toward Gaussian, but posteriors for  $F$  and  $c$  are right-skewed. Posteriors for parameter  $h$  appear somewhat uniform (HM1000, GBOED1000), slightly bimodal (GBOED200, BOED1000), or approximately normal (CES200, CES5400). Despite differences in posteriors, all methods were able to capture the true parameter values (denoted by black vertical lines in Figure 1). Note also that as the number of model evaluations increases, it may not necessarily be the case that the variance of the posterior distribution will decrease. As model evaluations increase, methods such as CES and GBOED especially may explore previously under-sampled regions of parameter space, leading to a more realistic representation of uncertainty.

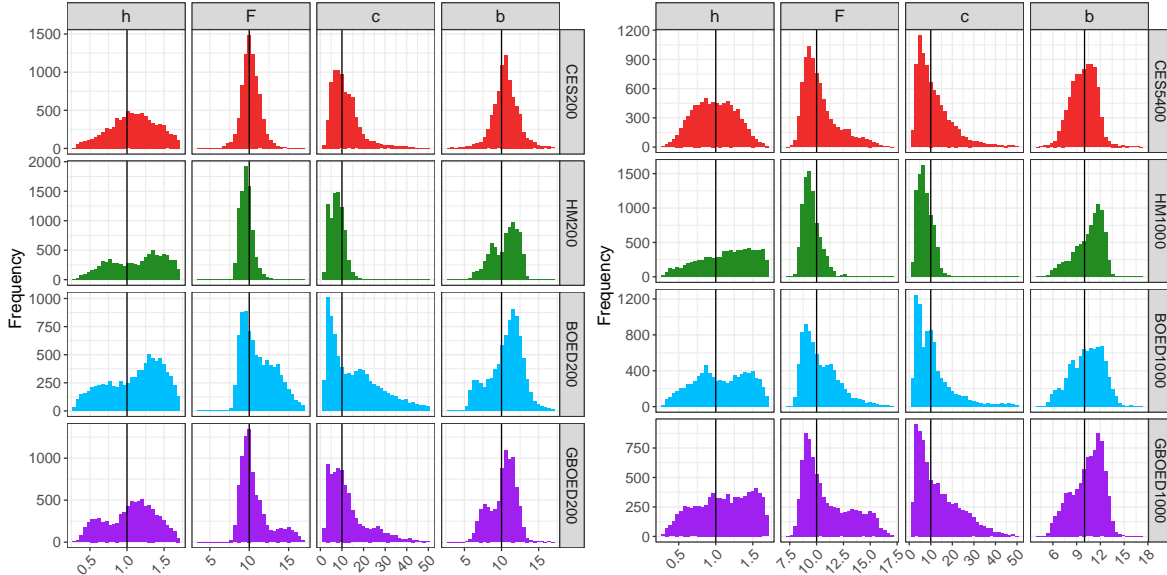


Figure 1: Frequency histograms of posterior distributions of parameters  $h$ ,  $F$ ,  $c$ , and  $b$  resulting from CES200, HM200, BOE200, and GBOED200 (left) and CES1000, HM1000, BOE1000, and GBOED1000 (right). Histograms represent 8192 values. True parameter values are denoted by vertical lines.

## 4.1 Convergence analysis

Next we conducted an exercise to gain insight into convergence rates of the main methods in calibrating the Lorenz '96 system. The goal of the convergence exercise was to determine how performance metrics of each method changed over increasing model evaluations. We report both score and AE every 100 evaluations up to 1000 total model evaluations for all methods. We included the intermediate (calibration) step of CES (EKS) as well for comparison.

AEs generally decreased as the number of model evaluations increased for parameter  $b$ , but there was considerable variability among methods for parameters  $h$ ,  $F$  and  $c$  (Figure 2, left panel). For instance, AEs for parameter  $c$  declined for methods BOED, CES, and EKS, but AEs increased markedly after 350 model evaluations for GBOED and were nearly constant for HM. In fact, AEs for GBOED consistently increased over model evaluations for all parameters, suggesting potential overfitting or instability.

For scores, the behavior varied by method. CES, EKS, BOED, and to some extent HM demonstrated slight but consistent improvements in score over increasing model evaluations (Figure 2, right panel). The stability of scores for HM over increasing model evaluations suggests that HM is less sensitive to the quantity of model evaluations once a sufficient baseline of information has been established. GBOED was unique in exhibiting a gradual decline in scores (degradation in performance) for all parameters over the 1000 model evaluations, which may be due to optimization quality and hyperparameter sensitivity (see SM3).

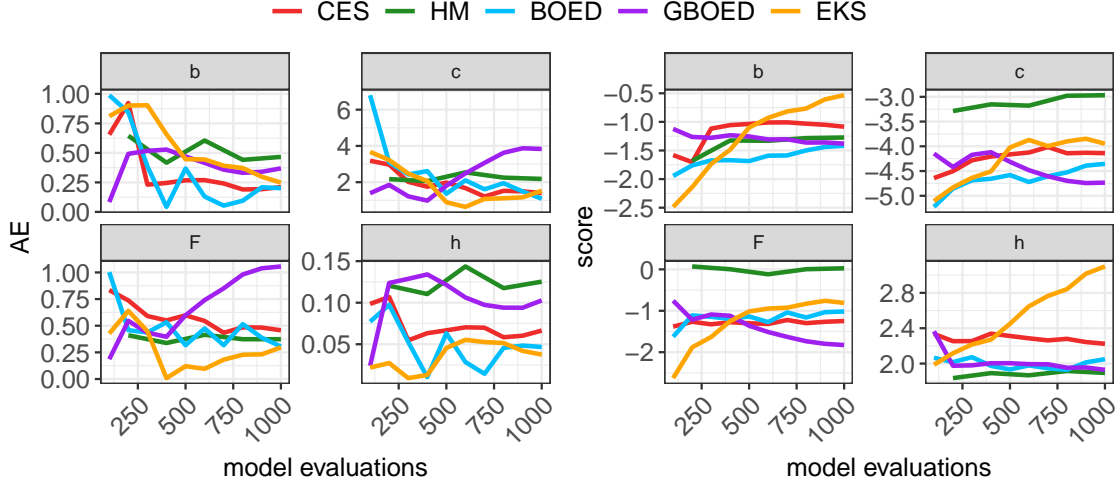


Figure 2: AEs (left) and scores (right) for CES, EKS, HM, BOED, and GBOED over increasing model evaluations for calibrating the Lorenz '96 system using base parameters  $\theta = (1, 10, 10, 10)$ .

This convergence analysis suggests that CES, GBOED, and HM may require as few as 500 model evaluations to achieve accurate parameter estimates with robust uncertainty quantification. However, the results also highlight important differences in behavior across methods. For example, while BOED and EKS appear to benefit from additional evaluations (with metrics continuing to improve at 1000 evaluations), GBOED performance may be hindered by excessive model evaluations.

Finally, it is important to note that these conclusions are based on a single set of true parameters for the Lorenz '96 system. The convergence behavior might differ for other parameter configurations, and future work should explore this sensitivity to provide a more comprehensive understanding of method performance across a variety of scenarios.

## 4.2 Performance evaluation

To obtain a fair and rigorous comparison of the main methods, we performed Bayesian inversion for  $\theta_i, i = 1 \dots 60$  using the Lorenz '96 multiscale system (Eq. 10). Each component of  $\theta_i$  was drawn from the following prior distributions based on baseline parameter values of 1, 10, log10, and 10 for  $h, F, c$ , and  $b$ , respectively:

$$\begin{aligned}
 h &\sim \text{Unif}(0.3, 7) \\
 F &\sim \text{Unif}(3, 17) \\
 c &\sim \text{Unif}(0.6908, 3.9144) \\
 b &\sim \text{Unif}(3, 17).
 \end{aligned}$$

Note that parameter  $c$  must be non-negative, so inversion for this parameter is performed in log space. Each component of  $\theta_i$  was drawn from a Uniform distribution with the minimum (maximum) being the baseline parameter value minus (plus) 70% of the baseline value. While

these priors are more constrained than the Gaussian priors used in [7], we found that Uniform prior distributions ensured stability of the system during calibration. Observables from this system ( $\phi_k(Z)$ ) and their associated variability ( $\Gamma_{obs}$ ) were computed for each  $\theta_i$  and were used within the MCMC sampling step included within all methods to obtain the posterior distribution for each  $\theta_i$ . We also compared the four main methods BOED, GBOED, CES, and HM against the following competitors:

- LHS200/2000: Posterior parameter distributions obtained via parameter values generated using a LHS design combined with MCMC. First, 200 (LHS200) or 1000 (LHS1000) LHS samples for parameters were generated. Next, the Lorenz '96 system was run using the LHS samples, and observed quantities  $\phi_K(Z)$  were computed for each of the 200 or 1000 samples. LHS parameter samples (inputs) and the observables (outputs) were used for GP emulator fitting. Finally, the fitted GPs, along with observables  $\phi_k(Z)$  and  $\Gamma_{obs}$  corresponding to each  $\theta_i$  were used to perform ST-MCMC sampling [4]. Including LHS-based methods as comparators allows us to determine if the calibration-specific steps of each method (e.g. EKS in CES) have added benefits.
- EKS200/5400: the posterior distribution resulting from EKS (the Calibrate step of CES). We include EKS, because, in contrast to other ensemble Kalman Filter methods such as EKI, it can provide systematic UQ during calibration [7]. We use the final iteration of EKS as the posterior distribution for calculating validation metrics. No MCMC sampling (and therefore no GP emulation) is required for EKS.

#### 4.2.1 Statistical analyses

To evaluate how well different methods performed, we constructed two linear, additive models: one for AE and another for score. The response for the models was either AE or score, and the two covariates were the type of method (e.g., BOED200, CES54000, etc) (*METHOD*) and parameters of the Lorenz '96 model ( $h, F, c, b$ ) (*PARAM*). Thus, *METHOD* and *PARAM* are factor-valued covariates with 11 and 4 levels, respectively. We considered AE and scores from the 60 calibration problems of the Lorenz '96 system as replicates in these models. The linear models for AE and score are thus two-way, additive analysis of variance (ANOVA) models with no interaction terms. We did not include interaction terms to preserve degrees of freedom, and preliminary analyses showed that interactions were not practically significant. The general form for both models can be expressed as:

$$y_{ijk} = \mu + \alpha_j + \beta_k + \epsilon_{ijk},$$

where  $y_{ijk}$  is the observation for the  $i$ th replicate,  $j$ th level of *METHOD* and the  $k$ th level of *PARAM*;  $\mu$  is the overall mean,  $\alpha_j$  and  $\beta_k$  are the effects of the  $j$ th level of *METHOD* and  $k$ th level of *PARAM*, respectively, and  $\epsilon_{ijk}$  is a normally distributed error term. The two ANOVA models for AE and score can be written more specifically as:

$$\begin{aligned} y_{ijk}^{AE} &= \beta_0 + \beta_1^{(METHOD_j)} + \beta_2^{(PARAM_k)} + \epsilon_{ijk}, \\ y_{ijk}^{SCORE} &= \beta_0 + \beta_1^{(METHOD_j)} + \beta_2^{(PARAM_k)} + \epsilon_{ijk}, \end{aligned} \tag{12}$$

where, in this formulation,  $\beta_1$  represents the effects of the 10 levels of *METHOD* relative to the *reference* level, and  $\beta_2$  represents the effects of the three levels of *PARAM* relative to the reference level. This model can be generally expressed in matrix form as  $\mathbf{Y} = \mathbf{X}\boldsymbol{\beta} + \boldsymbol{\epsilon}$ , where  $\mathbf{X}$  is a design matrix that encodes the levels of *METHOD* and *PARAM*. The coefficient vector  $\boldsymbol{\beta}$  contains ten coefficients for *METHOD*, three coefficients for *PARAM*, and one for the intercept. Additionally, we excluded extremely low score values (less than -50, primarily from LHS methods) from the dataset, as these could have disproportionately influenced the results. In total, 20 observations were removed. After fitting these models, we performed post-hoc pairwise comparisons of the estimated marginal means of AE by *METHOD* to determine if differences between any two calibration methods were significantly different. We applied the Bonferroni correction for post-hoc pairwise comparisons to control for family-wise error rate (FWER). While Tukey’s Honest Significant Difference (HSD) is commonly used for ANOVA post-hoc tests, it assumes equal group sizes, whereas Bonferroni remains valid for unequal sample sizes. Given our study design, Bonferroni provides a more conservative assessment of significant differences, which is what we desire. Significance of pairwise tests was assessed at  $\alpha = 0.05$ . All models were fitted in R using the `lm()` function [45]; pairwise comparisons were carried out using the `emmeans` [29] and `modelbased` [37] packages.

#### 4.2.2 Results

Overall, EKS5400 and GBOED200 outperformed all other methods with respect to AE and score for calibration of the Lorenz ’96 system. Most methods successfully estimated parameter  $h$  with a higher accuracy compared to parameters  $F$ ,  $c$  and  $b$  (Figure 3 A). The largest variability in performance was exhibited in parameter  $c$ , with AEs reaching values as high as 20 for some methods (Figure 3 A). LHS-based methods consistently underperformed in terms of both accuracy and UQ, emphasizing the limitations of relying solely on prior-based sampling without incorporating a calibration step (Figures 3 A and B).

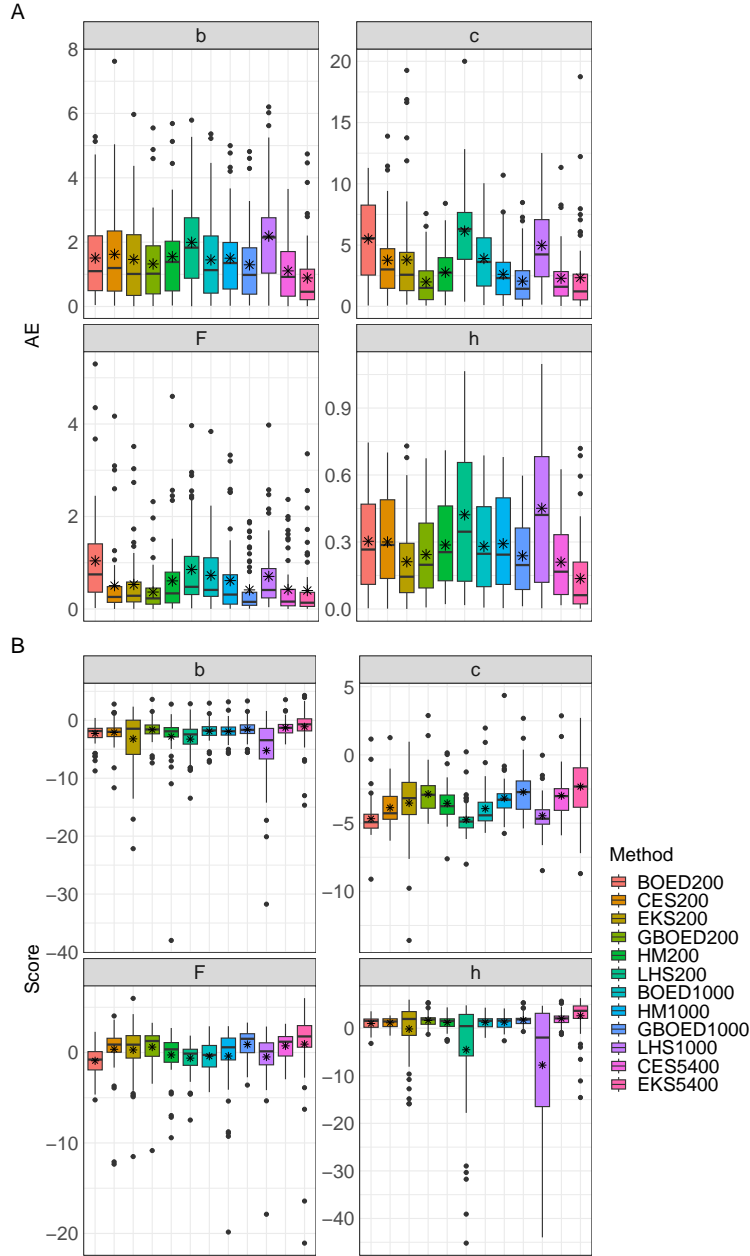


Figure 3: Boxplots of AEs (A) and log score (B) for calibrated parameters  $h$ ,  $F$ ,  $c$  and  $b$  of the Lorenz '96 model for all method. Each boxplot for AE represents 60 values; values less than -50 for score were omitted. AE values were calculated using the mean of the posterior distribution. Horizontal lines within boxplots represent the median, while stars denote means. Parameter  $c$  has been back-transformed from a log scale.

Pairwise comparisons of estimated marginal means of AE (averaged over all parameters) from the linear AE model (Eq. 12) revealed notable performance trends. LHS-based methods (LHS200, LHS1000) and BOED200 performed significantly worse than all other methods (Table 1, Figure 4). EKS5400 and GBOED200 outperformed six other methods including BOED200, BOED1000, CES200, EKS200, LHS200, and LHS1000 (Figure 4, Table

1). CES5400 and GBOED1000 also performed well but did not significantly outperform EKS200 (Table 1).

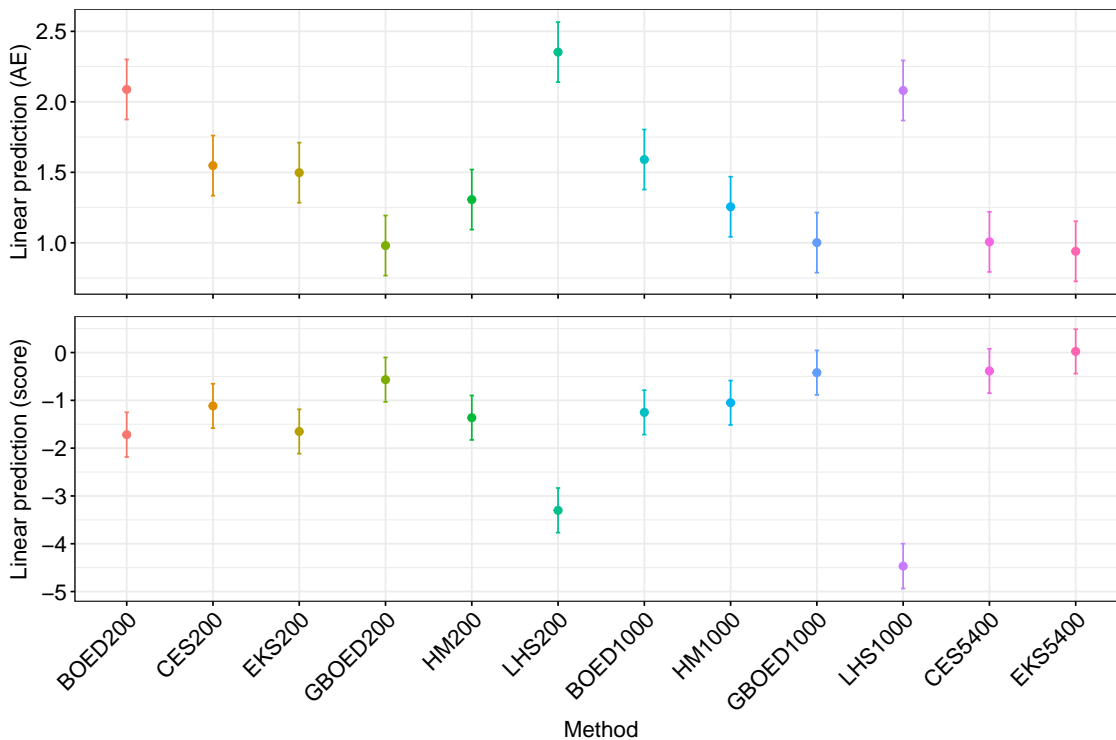


Figure 4: Estimated marginal means of absolute errors (AEs) (top) and score (bottom) averaged over the four parameters for the *AE* and *score* linear models described in Section 3.2. Error bars represent 95% confidence intervals (note that the confidence intervals reflect uncertainty around the estimated marginal means, not the raw data).

As suggested by the convergence analysis, the effect of increasing model evaluations varied by method. For CES and EKS, mean AEs decreased by approximately 50% from 200 to 5400 evaluations, and these differences were statistically significant (Table SM1), Figure 4). Similarly, BOED1000 achieved a 50% reduction in mean AE compared to BOED200, although this difference was not significant. In contrast, increasing model evaluations for HM and GBOED had little effect on AEs. Interestingly, GBOED200 achieved a slightly lower mean AE than GBOED1000 (Figure 4), reinforcing our earlier observation that additional model evaluations do not necessarily improve calibration performance for GBOED.

Out of the methods utilizing fewer evaluations (200), GBOED200 achieved the lowest mean AE and performed comparably to EKS5400. Among the methods with higher evaluation counts, EKS5400 achieved the lowest mean AE (Figure 4). All pairwise comparisons from the linear AE model are provided in SM2, SM1.

Results for score were largely consistent with those for AE, with some notable differences. Like results for AE, LHS200 and LHS1000 had significantly worse (lower) scores compared to all other methods (Table 1, Figure 4). Notably, LHS-based methods were the only ones with extreme score outliers (-100 or less). This finding emphasizes the importance of an

initial calibration step to achieve robust UQ. EKS5400 again achieved the highest mean score, significantly outperforming six methods: LHS200, LHS1000, BOED200, BOED1000, EKS200, and CES200. GBOED1000 outperformed five methods, while CES5400 and GBOED200 ranked similarly, outperforming four methods each (Table 1). All pairwise comparisons based on the linear model for score can be found in SM2, Table SM2.

Unlike the results for AE, increasing the number of model evaluations for GBOED slightly *improved* UQ. Although BOED methods generally underperformed, they achieved significantly better scores than LHS-based methods. Finally, while HM methods had fair performance in parameter estimation accuracy, significantly outperforming four methods, their performance in UQ was limited to outperforming only the LHS-based methods (Table 1).

Table 1: Methods in the *leftmost* column have significantly lower (better) mean AE values than those in the middle column (AE) and significantly higher (better) scores than those in the rightmost column (Score) at  $\alpha = 0.05$ . For example, the estimated marginal mean AE of EKS200 in the leftmost column is significantly lower than mean AEs of BOED200, LHS200, and LHS1000 in the middle column. Significant differences are based on pairwise comparisons from the linear models for AE and score (Eq. 12).

Method	AE	Score
BOED200	none	LHS200, LHS1000
BOED1000	LHS200	LHS200, LHS1000
CES5400	BOED1000, BOED 200, CES200, LHS200, LHS1000	BOED1000, EKS200, LHS200, LHS1000
CES200	LHS200, LHS1000	LHS200, LHS1000
EKS5400	BOED1000, BOED200, CES200, EKS200, LHS200, LHS1000	BOED1000, BOED200, CES200, EKS200, LHS200, LHS1000
EKS200	BOED200, LHS200, LHS1000	LHS200, LHS1000
GBOED1000	BOED1000, BOED200, CES200, LHS200, LHS1000	BOED1000, BOED200, CES200, LHS200, LHS1000
GBOED200	BOED1000, BOED200, CES200, EKS200, LHS200, LHS1000	BOED200, BOED1000, LHS200, LHS1000
HM200	BOED200, BOED1000, LHS200, LHS1000	LHS200, LHS1000
HM1000	BOED200, BOED1000, LHS200, LHS1000	LHS200, LHS1000
LHS200	none	LHS1000
LHS1000	none	none

## 5 Discussion and conclusions

In this study, we compared four Bayesian calibration methods (BOED, GBOED, HM, CES) along with EKS (the “Calibration” step of CES) and naive LHS-based methods for calibrating the Lorenz ’96 multiscale system. Our study provides a rigorous comparison of traditional methods for solving inverse problems (CES, HM) and less commonly used methods like BOED and GBOED. Each method was tested with both a limited number (200) and a larger number

(1000–5400) of model evaluations. Additionally, we conducted a convergence analysis to understand how performance metrics evolved as the number of model evaluations increased.

Our results highlight several key insights. Traditional methods, particularly CES and its built-in calibration method EKS, performed exceptionally well in calibrating the Lorenz '96 system. EKS slightly outperformed CES in both accuracy and UQ when using a large number (5400) of model evaluations. GBOED exhibited comparable performance to EKS in accuracy and uncertainty quantification. BOED, however, generally underperformed relative to GBOED, CES, HM, and EKS, suggesting that its design may not be well-suited to the emulator-based calibration problem as implemented here. This may be because an emulator like a GP does not generalize well far from training data so it is important to have many samples in calibration-relevant regions, which motivates the use of goal-oriented methods. HM performed reasonably well and could serve as an initial refinement of the parameter space during calibration. With a limited set of model evaluations, HM can significantly refine the parameter space and could be used as a precursor to other methods such as CES. Such an approach is especially advantageous when computational resources are limited and information about the underlying system is unknown, as it avoids wasting evaluations on implausible regions.

Our paper is one of the first to apply BOED-based methods to climate model calibration, following the earlier study by [12]. In [12] BOED was integrated into CES to guide design choices for improving seasonal time-averaged statistics through calibration. In our implementation of BOED and GBOED, the “calibration” step is already embedded within the BOED and GBOED algorithms. An interesting extension of this work could involve integrating GBOED (which outperformed BOED) into CES, potentially leveraging the strengths of both methods. The underwhelming performance of BOED may also stem from our test system, the Lorenz '96 system, such as its relatively small parameter space or the simplicity of the problem. Alternatively, BOED’s performance may depend on choices in its implementation, such as prior distributions, emulator fitting, or the number of evaluations used for KL divergence calculations. These aspects warrant further investigation.

While GBOED demonstrated excellent performance with as few as 200 model evaluations, it came at the expense of significant computational costs. For instance, running GBOED for 1000 evaluations required approximately a week to complete on an HPC system. This high computational burden is primarily due to the repeated evaluation of the KL divergence, as well as the intermediate sampling steps required to optimize the Expected Information Gain (EIG). The additional complexity arises from the nested optimization loops and the need to repeatedly fit and query the GP emulator. Additionally, we observed mixed results for GBOED’s performance as model evaluations increased. Our comprehensive performance assessment showed that while its accuracy slightly decreased, its UQ marginally improved when model evaluations increased from 200 to 1000. This suggests that GBOED may benefit from tuning specific elements of its setup, such as the choice of priors or emulator fitting. Given its high computational cost, we do not recommend using GBOED for more than 200 evaluations unless specific computational resources or improvements in implementation efficiency are available.

Our findings also differ somewhat from those of [7], who showed that CES better characterized parameter uncertainty for the Lorenz '96 system compared to EKS. In contrast, we found that EKS outperformed CES in both accuracy and UQ for the same system. While we

implemented CES based on methods described in [7], differences in sampling or emulation steps may explain the discrepancy. For larger, more computationally intensive problems, performing as many evaluations as we did for EKS (e.g., 5400) is generally not feasible. In such cases, CES would offer a significant advantage due to its efficient integration of the calibration, emulation, and sampling steps. For smaller problems, however, EKS appears to be sufficient and is simpler to implement because it requires neither emulator fitting nor MCMC sampling.

Overall, this study provides valuable insights into the strengths and limitations of various Bayesian calibration methods. While traditional methods like EKS and CES perform reliably, GBOED shows promise as a non-traditional OED approach for calibration, it requires further optimization to manage its computational cost. BOED, while underperforming here, may still hold potential in other contexts with different implementation choices or problem complexities. Finally, while HM exhibited fair performance on its own, it could be used as a precursor to other methods. Future work should explore the performance of these methods on more complex systems, as well as investigate how implementation details affect results.

## Data and code availability

All code and data used for this study is available in a Zenodo repository:  
<https://zenodo.org/records/13761230>.

## Acknowledgments

We would like to thank early reviewers for improving our manuscript.

## References

- [1] A. ATTIA, A. ALEXANDERIAN, AND A. K. SAIBABA, *Goal-oriented optimal design of experiments for large-scale Bayesian linear inverse problems*, Inverse Problems, 34 (2018), p. 095009.
- [2] J. M. BERNARDO, *Expected information as expected utility*, the Annals of Statistics, (1979), pp. 686–690.
- [3] M. BOCQUET, *Surrogate modeling for the climate sciences dynamics with machine learning and data assimilation*, Frontiers in Applied Mathematics and Statistics, 9 (2023), <https://doi.org/10.3389/fams.2023.1133226>, <https://www.frontiersin.org/articles/10.3389/fams.2023.1133226>.
- [4] T. A. CATANACH, H. D. VO, AND B. MUNSKY, *Bayesian inference of stochastic reaction networks using multifidelity sequential tempered Markov Chain Monte Carlo*, International journal for uncertainty quantification, 10 (2020).
- [5] K. CHALONER AND I. VERDINELLI, *Bayesian experimental design: A review*, Statistical science, (1995), pp. 273–304.

- [6] W. CHANG, M. HARAN, R. OLSON, AND K. KELLER, *Fast dimension-reduced climate model calibration and the effect of data aggregation*, The Annals of Applied Statistics, 8 (2014).
- [7] E. CLEARY, A. GARBUNO-INIGO, S. LAN, T. SCHNEIDER, AND A. M. STUART, *Calibrate, emulate, sample*, Journal of Computational Physics, 424 (2021), p. 109716.
- [8] F. COUVREUX, F. HOURDIN, D. WILLIAMSON, R. ROEHRIG, V. VOLODINA, N. VILLEFRANQUE, C. RIO, O. AUDOUIN, J. SALTER, E. BAZILE, ET AL., *Process-based climate model development harnessing machine learning: I. a calibration tool for parameterization improvement*, Journal of Advances in Modeling Earth Systems, 13 (2021), p. e2020MS002217.
- [9] P. S. CRAIG, M. GOLDSTEIN, A. H. SEHEULT, AND J. A. SMITH, *Pressure matching for hydrocarbon reservoirs: a case study in the use of Bayes linear strategies for large computer experiments*, in Case Studies in Bayesian Statistics: Volume III, Springer, 1997, pp. 37–93.
- [10] C. DROVANDI, D. J. NOTT, AND D. E. PAGENDAM, *A semiautomatic method for history matching using sequential Monte Carlo*, SIAM/ASA Journal on Uncertainty Quantification, 9 (2021), pp. 1034–1063, <https://doi.org/10.1137/19M1286694>, <https://doi.org/10.1137/19M1286694>, <https://arxiv.org/abs/https://doi.org/10.1137/19M1286694>.
- [11] O. R. DUNBAR, A. GARBUNO-INIGO, T. SCHNEIDER, AND A. M. STUART, *Calibration and uncertainty quantification of convective parameters in an idealized gcm*, Journal of Advances in Modeling Earth Systems, 13 (2021), p. e2020MS002454.
- [12] O. R. DUNBAR, M. F. HOWLAND, T. SCHNEIDER, AND A. M. STUART, *Ensemble-based experimental design for targeting data acquisition to inform climate models*, Journal of Advances in Modeling Earth Systems, 14 (2022), p. e2022MS002997.
- [13] O. R. A. DUNBAR, A. GARBUNO-INIGO, T. SCHNEIDER, AND A. M. STUART, *Calibration and Uncertainty Quantification of Convective Parameters in an Idealized GCM*, Journal of Advances in Modeling Earth Systems, 13 (2021), p. e2020MS002454, <https://doi.org/https://doi.org/10.1029/2020MS002454>, <https://agupubs.onlinelibrary.wiley.com/doi/abs/10.1029/2020MS002454>, <https://arxiv.org/abs/https://agupubs.onlinelibrary.wiley.com/doi/pdf/10.1029/2020MS002454>. e2020MS002454 2020MS002454.
- [14] J. P. DUNNE, L. W. HOROWITZ, A. J. ADCROFT, P. GINOX, I. M. HELD, J. G. JOHN, J. P. KRASTING, S. MALYSHEV, V. NAIK, F. PAULOT, E. SHEVLIKOVA, C. A. STOCK, N. ZADEH, V. BALAJI, C. BLANTON, K. A. DUNNE, C. DUPUIS, J. DURACHTA, R. DUSSIN, P. P. G. GAUTHIER, S. M. GRIFFIES, H. GUO, R. W. HALLBERG, M. HARRISON, J. HE, W. HURLIN, C. MCHUGH, R. MENZEL, P. C. D. MILLY, S. NIKONOV, D. J. PAYNTER, J. PLOSHAY, A. RADHAKRISHNAN, K. RAND, B. G. REICHL, T. ROBINSON, D. M. SCHWARZKOPF, L. T.

- SENTMAN, S. UNDERWOOD, H. VAHLENKAMP, M. WINTON, A. T. WITTENBERG, B. WYMAN, Y. ZENG, AND M. ZHAO, *The GFDL Earth System Model Version 4.1 (GFDL-ESM 4.1): Overall Coupled Model Description and Simulation Characteristics*, Journal of Advances in Modeling Earth Systems, 12 (2020), p. e2019MS002015, <https://doi.org/https://doi.org/10.1029/2019MS002015>, <https://agupubs.onlinelibrary.wiley.com/doi/abs/10.1029/2019MS002015>, <https://arxiv.org/abs/https://agupubs.onlinelibrary.wiley.com/doi/pdf/10.1029/2019MS002015>. e2019MS002015 2019MS002015.
- [15] O. DÜRR, P.-Y. FAN, AND Z.-X. YIN, *Bayesian calibration of mems accelerometers*, IEEE Sensors Journal, 23 (2023), pp. 13319–13326.
- [16] N. R. EDWARDS, D. CAMERON, AND J. ROUGIER, *Precalibrating an intermediate complexity climate model*, Climate dynamics, 37 (2011), pp. 1469–1482.
- [17] C. EHRETT, D. A. BROWN, C. KITCHENS, X. XU, R. PLATZ, AND S. ATAMTURKUR, *Simultaneous Bayesian calibration and engineering design with an application to a vibration isolation system*, Journal of Verification, Validation and Uncertainty Quantification, 6 (2021), p. 011007.
- [18] A. R. FERROLINO, J. E. C. LOPE, AND R. G. MENDOZA, *Optimal location of sensors for early detection of tsunami waves*, in Computational Science–ICCS 2020: 20th International Conference, Amsterdam, The Netherlands, June 3–5, 2020, Proceedings, Part II 20, Springer, 2020, pp. 562–575.
- [19] A. GARBUNO-INIGO, F. HOFFMANN, W. LI, AND A. M. STUART, *Interacting Langevin diffusions: Gradient structure and ensemble Kalman sampler*, SIAM Journal on Applied Dynamical Systems, 19 (2020), pp. 412–441.
- [20] J. GINEBRA, *On the measure of the information in a statistical experiment*, Bayesian Analysis, 2 (2007), pp. 167–212.
- [21] T. GNEITING AND A. E. RAFTERY, *Strictly proper scoring rules, prediction, and estimation*, Journal of the American statistical Association, 102 (2007), pp. 359–378.
- [22] R. B. GRAMACY, *Surrogates: Gaussian process modeling, design, and optimization for the applied sciences*, Chapman and Hall/CRC, 2020.
- [23] L. M. HELLECKES, M. OSTHEGE, W. WIECHERT, E. VON LIERES, AND M. OLDIGES, *Bayesian calibration, process modeling and uncertainty quantification in biotechnology*, PLoS computational biology, 18 (2022), p. e1009223.
- [24] C. S. JACKSON, M. K. SEN, G. HUERTA, Y. DENG, AND K. P. BOWMAN, *Error reduction and convergence in climate prediction*, Journal of Climate, 21 (2008), pp. 6698–6709.
- [25] S. JAIN, A. A. SCAIFE, T. G. SHEPHERD, C. DESER, N. DUNSTONE, G. A. SCHMIDT, K. E. TRENBERTH, AND T. TURKINGTON, *Importance of internal variability for climate model assessment*, npj Climate and Atmospheric Science, 6 (2023), p. 68.

- [26] M. C. KENNEDY AND A. O’HAGAN, *Bayesian calibration of computer models*, Journal of the Royal Statistical Society: Series B (Statistical Methodology), 63 (2001), pp. 425–464.
- [27] R. C. KING, L. A. MANSFIELD, AND A. SHESHADRI, *Bayesian history matching applied to the calibration of a gravity wave parameterization*, Journal of Advances in Modeling Earth Systems, 16 (2024), p. e2023MS004163.
- [28] N. B. KOVACHKI AND A. M. STUART, *Ensemble Kalman inversion: a derivative-free technique for machine learning tasks*, Inverse Problems, 35 (2019), p. 095005.
- [29] R. V. LENTH, *emmeans: Estimated Marginal Means, aka Least-Squares Means*, 2024, <https://CRAN.R-project.org/package=emmeans>. R package version 1.10.5.
- [30] L. R. LEUNG, D. C. BADER, M. A. TAYLOR, AND R. B. MCCOY, *An Introduction to the E3SM Special Collection: Goals, Science Drivers, Development, and Analysis*, Journal of Advances in Modeling Earth Systems, 12 (2020), p. e2019MS001821, <https://doi.org/https://doi.org/10.1029/2019MS001821>, <https://agupubs.onlinelibrary.wiley.com/doi/abs/10.1029/2019MS001821>, <https://arxiv.org/abs/https://agupubs.onlinelibrary.wiley.com/doi/pdf/10.1029/2019MS001821>. e2019MS001821 2019MS001821.
- [31] R. LGUENSAT, J. DESHAYES, H. DURAND, AND V. BALAJI, *Semi-automatic tuning of coupled climate models with multiple intrinsic timescales: Lessons learned from the Lorenz 96 model*, Journal of Advances in Modeling Earth Systems, 15 (2023), p. e2022MS003367.
- [32] R. LGUENSAT, J. DESHAYES, H. DURAND, AND V. BALAJI, *Semi-automatic tuning of coupled climate models with multiple intrinsic timescales: Lessons learned from the lorenz96 model*, Journal of Advances in Modeling Earth Systems, 15 (2023), p. e2022MS003367, <https://doi.org/https://doi.org/10.1029/2022MS003367>, <https://agupubs.onlinelibrary.wiley.com/doi/abs/10.1029/2022MS003367>, <https://arxiv.org/abs/https://agupubs.onlinelibrary.wiley.com/doi/pdf/10.1029/2022MS003367>. e2022MS003367 2022MS003367.
- [33] D. V. LINDLEY, *On a measure of the information provided by an experiment*, The Annals of Mathematical Statistics, 27 (1956), pp. 986–1005.
- [34] Y. LING AND S. MAHADEVAN, *Challenging issues in bayesian calibration of multi-physics models*, in 54th AIAA/ASME/ASCE/AHS/ASC Structures, Structural Dynamics, and Materials Conference, 2013, p. 1874.
- [35] E. N. LORENZ, *Predictability: A problem partly solved*, in Proc. Seminar on predictability, vol. 1, Reading, 1996.
- [36] N. LUTSKO, B. CORNUELLE, S. GILLE, M. MAZLOFF, AND M. MORZFELD, *Machine learning for surrogate modeling of the upper ocean and heat exchange between the ocean and atmosphere*, (2021), <https://doi.org/10.2172/1769742>, <https://www.osti.gov/biblio/1769742>.

- [37] D. MAKOWSKI, M. S. BEN-SHACHAR, I. PATIL, AND D. LÜDECKE, *Estimation of model-based predictions, contrasts and means.*, CRAN, (2020), <https://github.com/easystats/modelbased>.
- [38] M. D. MCKAY, R. J. BECKMAN, AND W. J. CONOVER, *A comparison of three methods for selecting values of input variables in the analysis of output from a computer code*, *Technometrics*, 21 (1979), pp. 239–245, <http://www.jstor.org/stable/1268522> (accessed 2024-10-16).
- [39] L. NOVAK AND D. NOVAK, *Polynomial chaos expansion for surrogate modelling: Theory and software*, *Beton-und Stahlbetonbau*, 113 (2018), pp. 27–32.
- [40] D. ORRELL, *Model error and predictability over different timescales in the Lorenz’96 systems*, *Journal of the atmospheric sciences*, 60 (2003), pp. 2219–2228.
- [41] E. OTT, B. R. HUNT, I. SZUNYOGH, A. V. ZIMIN, E. J. KOSTELICH, M. CORAZZA, E. KALNAY, D. PATIL, AND J. A. YORKE, *A local ensemble Kalman filter for atmospheric data assimilation*, *Tellus A: Dynamic Meteorology and Oceanography*, 56 (2004), pp. 415–428.
- [42] A. B. OWEN, *Quasi-Monte Carlo Sampling*, *Monte Carlo Ray Tracing: Siggraph*, 1 (2003), pp. 69–88.
- [43] R. PARTHIPAN, H. M. CHRISTENSEN, J. S. HOSKING, AND D. J. WISCHIK, *Using probabilistic machine learning to better model temporal patterns in parameterizations: a case study with the Lorenz 96 model*, *Geoscientific Model Development*, 16 (2023), pp. 4501–4519.
- [44] F. PUKELSHEIM, *The three sigma rule*, *The American Statistician*, 48 (1994), pp. 88–91, <http://www.jstor.org/stable/2684253> (accessed 2024-09-17).
- [45] R CORE TEAM, *R: A Language and Environment for Statistical Computing*, R Foundation for Statistical Computing, Vienna, Austria, 2023, <https://www.R-project.org/>.
- [46] J. RAÄISAÄNEN, *How reliable are climate models?*, *Tellus A: Dynamic Meteorology and Oceanography*, 59 (2007), pp. 2–29.
- [47] N. RAOULT, S. BEYLAT, J. M. SALTER, F. HOURDIN, V. BASTRIKOV, C. OTTLÉ, AND P. PEYLIN, *Exploring the potential of history matching for land surface model calibration*, *Geoscientific Model Development*, 17 (2024), pp. 5779–5801.
- [48] D. E. RICCIARDI, D. T. SEIDL, B. T. LESTER, A. R. JONES, AND E. JONES, *Bayesian optimal experimental design for constitutive model calibration*, *International Journal of Mechanical Sciences*, 265 (2024), p. 108881.
- [49] E. SEBOK, H. J. HENRIKSEN, E. PASTÉN-ZAPATA, P. BERG, G. THIREL, A. LEMOINE, A. LIRA-LOARCA, C. PHOTIADOU, R. PIMENTEL, P. ROYER-GASPARD, ET AL., *Use of expert elicitation to assign weights to climate and hydrological models in climate impact studies*, *Hydrology and Earth System Sciences*, 26 (2022), pp. 5605–5625.

- [50] C. SMITH, D. P. CUMMINS, H.-B. FREDRIKSEN, Z. NICHOLLS, M. MEINSHAUSEN, M. ALLEN, S. JENKINS, N. LEACH, C. MATHISON, AND A.-I. PARTANEN, *Fair-calibrate v1. 4.1: calibration, constraining, and validation of the fair simple climate model for reliable future climate projections*, Geoscientific Model Development, 17 (2024), pp. 8569–8592.
- [51] A. SOKOLOV, D. KICKLIGHTER, A. SCHLOSSER, C. WANG, E. MONIER, B. BROWN-STEINER, R. PRINN, C. FOREST, X. GAO, A. LIBARDONI, AND S. EASTHAM, *Description and Evaluation of the MIT Earth System Model (MESM)*, Journal of Advances in Modeling Earth Systems, 10 (2018), pp. 1759–1789, <https://doi.org/https://doi.org/10.1029/2018MS001277>, <https://agupubs.onlinelibrary.wiley.com/doi/abs/10.1029/2018MS001277>, <https://arxiv.org/abs/https://agupubs.onlinelibrary.wiley.com/doi/pdf/10.1029/2018MS001277>.
- [52] M. STUTE, A. CLEMENT, AND G. LOHMANN, *Global climate models: Past, present, and future*, Proceedings of the National Academy of Sciences, 98 (2001), pp. 10529–10530.
- [53] F. A. VIANA AND A. K. SUBRAMANIYAN, *A survey of Bayesian calibration and physics-informed neural networks in scientific modeling*, Archives of Computational Methods in Engineering, 28 (2021), pp. 3801–3830.
- [54] T. WEBER, A. COROTAN, B. HUTCHINSON, B. KRAVITZ, AND R. LINK, *Technical note: Deep learning for creating surrogate models of precipitation in Earth system models*, Atmospheric Chemistry and Physics, 20 (2020), pp. 2303–2317, <https://doi.org/10.5194/acp-20-2303-2020>, <https://acp.copernicus.org/articles/20/2303/2020/>.
- [55] C. K. WILLIAMS AND C. E. RASMUSSEN, *Gaussian processes for machine learning*, vol. 2, MIT press Cambridge, MA, 2006.
- [56] D. WILLIAMSON, A. T. BLAKER, C. HAMPTON, AND J. SALTER, *Identifying and removing structural biases in climate models with history matching*, Climate dynamics, 45 (2015), pp. 1299–1324.
- [57] D. WILLIAMSON, M. GOLDSTEIN, L. ALLISON, A. BLAKER, P. CHALLENGOR, L. JACKSON, AND K. YAMAZAKI, *History matching for exploring and reducing climate model parameter space using observations and a large perturbed physics ensemble*, Climate dynamics, 41 (2013), pp. 1703–1729.
- [58] K. WU, P. CHEN, AND O. GHATTAS, *An efficient method for goal-oriented linear Bayesian optimal experimental design: Application to optimal sensor placement*, arXiv preprint arXiv:2102.06627, (2021).
- [59] D. YARGER, B. M. WAGMAN, K. CHOWDHARY, AND L. SHAND, *Autocalibration of the e3sm version 2 atmosphere model using a PCA-based surrogate for spatial fields*, Journal of Advances in Modeling Earth Systems, 16 (2024), p. e2023MS003961.

- [60] S. ZHONG, W. SHEN, T. CATANACH, AND X. HUAN, *Goal-oriented Bayesian optimal experimental design for nonlinear models using markov chain monte carlo*, arXiv preprint arXiv:2403.18072, (2024).